Table S1 The calculated equilibrium lattice parameters (a), the layer thicknesses (L), the bond lengths between surface M atom and termination ($d_{M\text{-}T}$), the differences of adsorption energy between the configuration I and configuration II ($\Delta E_{\mathbf{adsorption}} = E_{\mathbf{configuration\ I}} - E_{\mathbf{configuration\ II}}$), and the band gaps ($\Delta E_{gap}$) of the selected oxygen-functionalized MXenes in comparison with previous theoretical results.

Material		a (Å)	L (Å)	$d_{M\text{-}T}$ (Å)	$\Delta E_{adsorption}$ (eV)	ΔE_{gap} (eV)
I-Ti_2CO_2	Theo.[a.]	3.0349	4.47	1.98	0.88	0.24
	Theo.[b.]	3.029	4.45	1.98	0.88	0.24
	Theo.[c.]					0.25
	Theo.[d.]	3.04				0.26
	PBE	3.0330	4.46	1.98	0.88	0.25
II-Mo_2CO_2	Theo.[e.]	2.8836	5.21	2.07	-0.55	metallic
	Theo.[f.]	2.891			-0.65	metallic
	Theo.[g.]				-0.56	metallic
	PBE	2.8828	5.20	2.07	-0.55	metallic

[a.] Ref. 1, [b.] Ref. 2, [c.] Ref. 3, [d.] Ref. 4, [e.] Ref. 5, [f.] Ref. 6, [g.] Ref. 7.

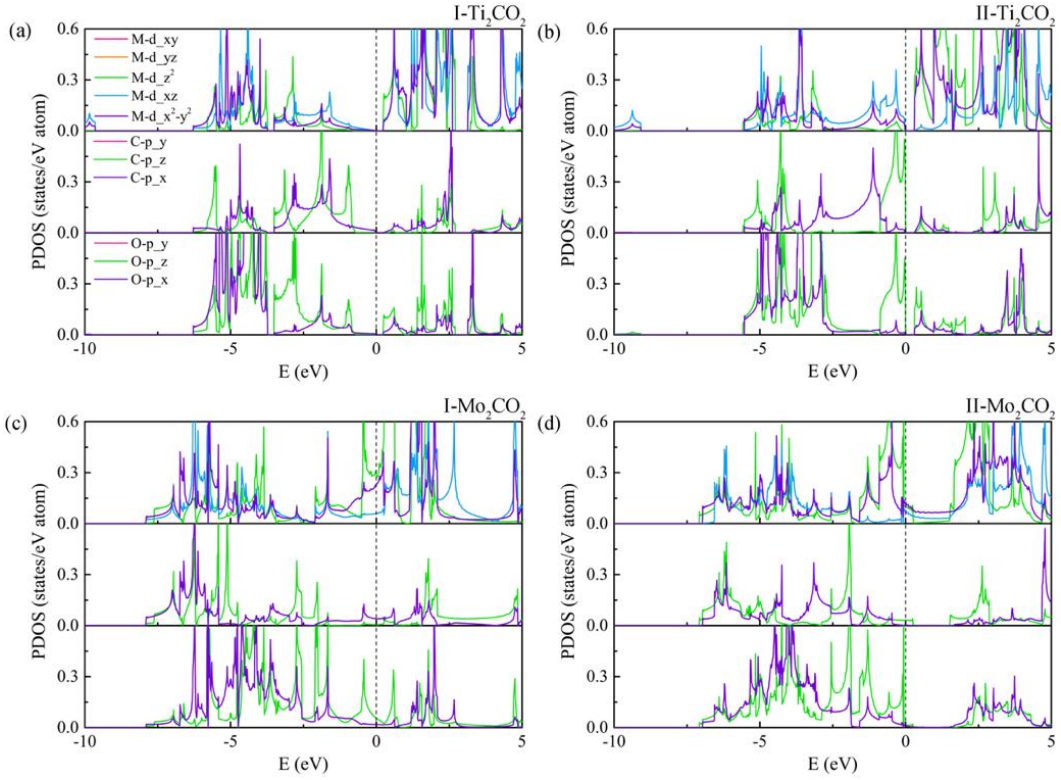

Fig. S1 The PDOS of (a) I-Ti_2CO_2, (b) II-Ti_2CO_2, (c) I-Mo_2CO_2 and (d) II-Mo_2CO_2. The Fermi level is set to zero.

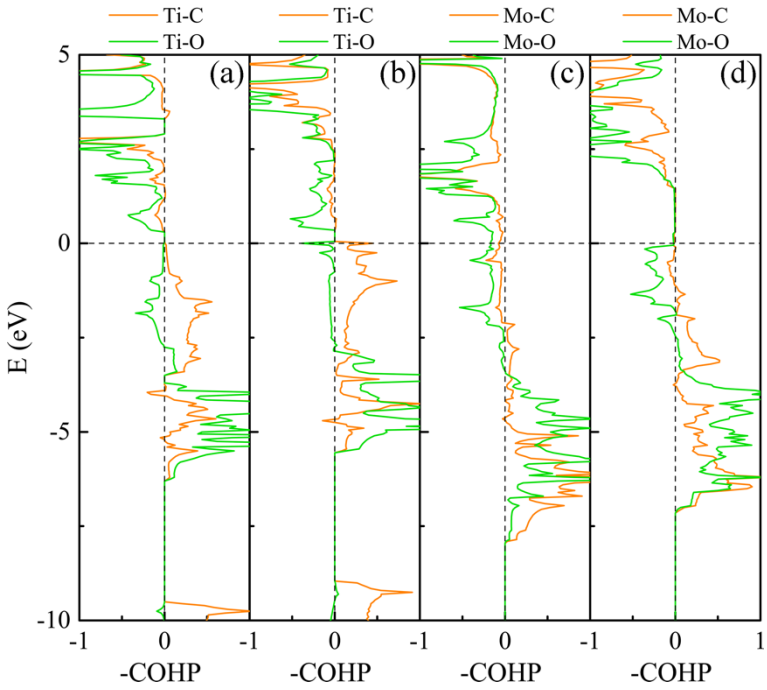

Fig. S2 The COHP analyses of (a) I-Ti_2CO_2, (b) II-Ti_2CO_2, (c) I-Mo_2CO_2 and (d) II-Mo_2CO_2. The Fermi level is set to zero.

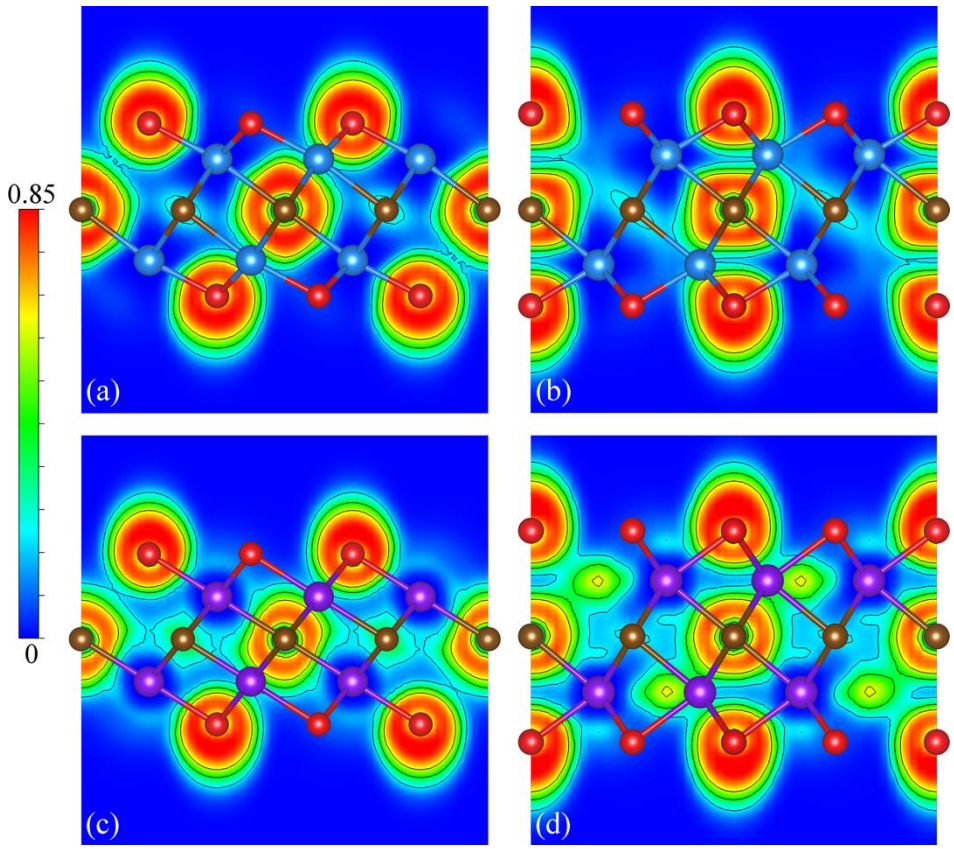

Fig. S3 The ELF maps of (a) I-Ti_2CO_2, (b) II-Ti_2CO_2, (c) I-Mo_2CO_2 and (d) II-Mo_2CO_2.

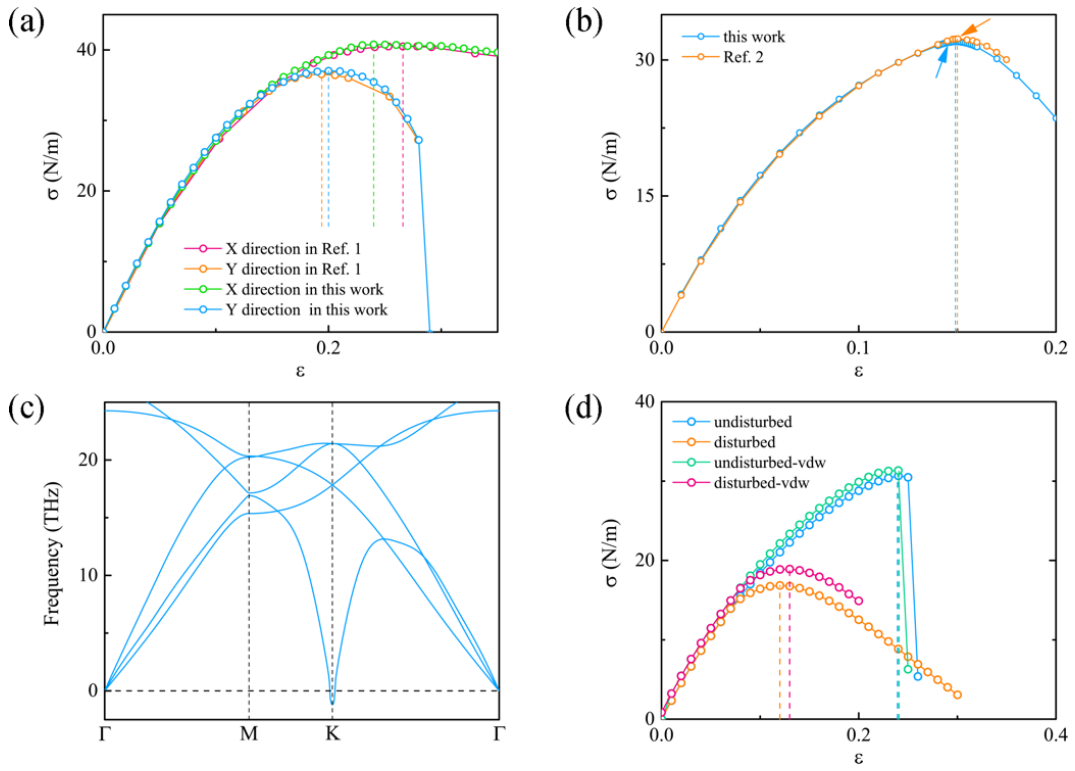

Fig. S4 (a) The stress-strain curves of graphene under uniaxial tension along *X* direction and *Y* direction, in excellent agreement with the previous results[8]. (b) The stress-strain curves of graphene under biaxial tension, in agreement with the results of Si et al.[9] (c) the lower phonon dispersion of graphene at $\varepsilon = 14.5\%$. (d) The comparison of the stress-strain curves of Ti_2CO_2 in the original PBE functional and the revised optB86b-vdW functional under uniaxial tension along *X* direction.

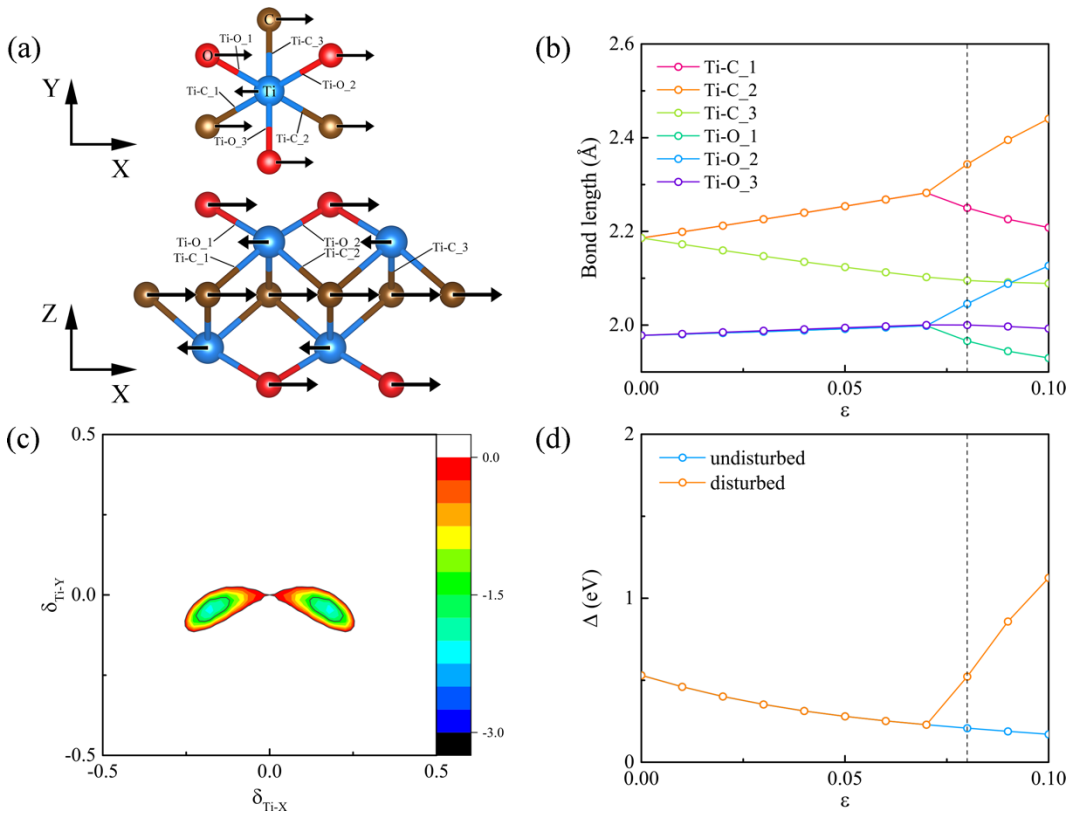

Fig. S5 (a) The imaginary eigenvector in top view and in side view and (c) the energy vs in-plane movements of a Ti atom at ε = 0.15 under uniaxial tension along X direction. Note that the unit in the energy map is meV. (b) The bond length vs strain (ε) curve and (d) the gap at Γ point (Δ) vs strain (ε) curve of Ti_2CO_2 under uniaxial tension along X direction. Note that the dot lines indicate the appearance of phonon instability.

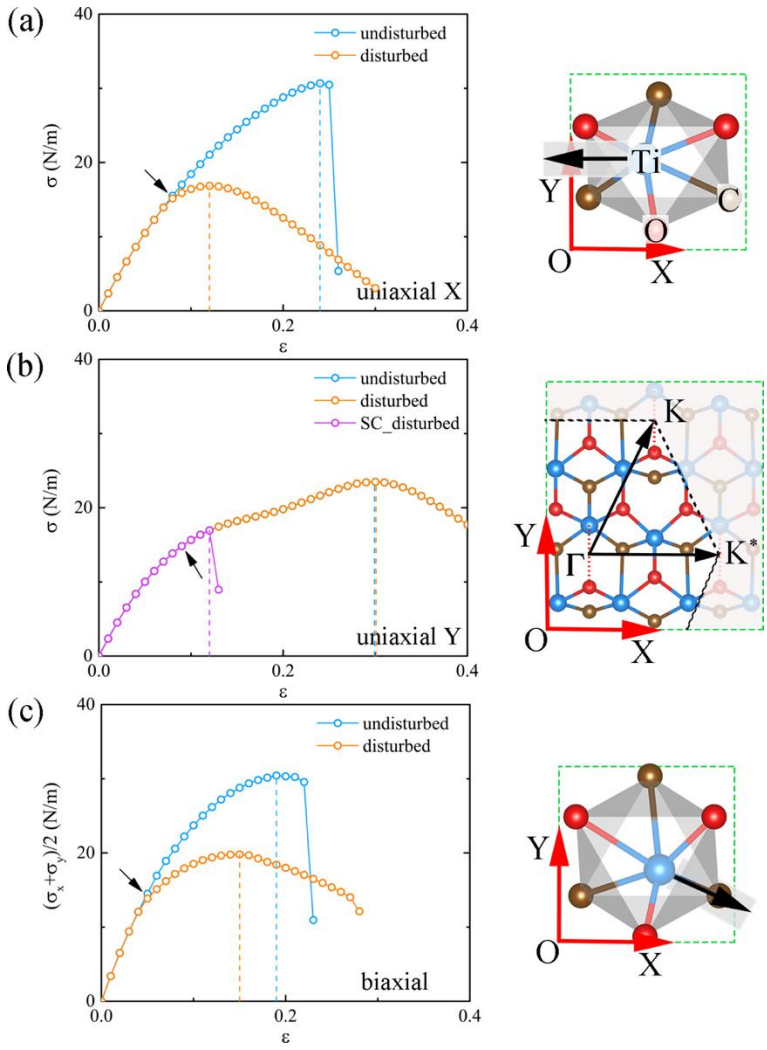

Fig. S6 The calculated stress-strain curves of Ti_2CO_2 under uniaxial tension along (a) *X* direction and (b) *Y* direction, and (c) under biaxial tension, respectively. Note that the words "undisturbed" and "disturbed" represent that the undisturbed and disturbed methods, respectively. "SC_disturbed" stands for the calculation performed for a supercell of 2×2×1 by the disturbed method. Note that the undisturbed curve and disturbed one are perfectly superimposed in Fig. S6b. The arrows indicate the appearance of dynamic instabilities. The right panels show the deformed polyhedral structure of Ti_2CO_2 under the corresponding strain states.

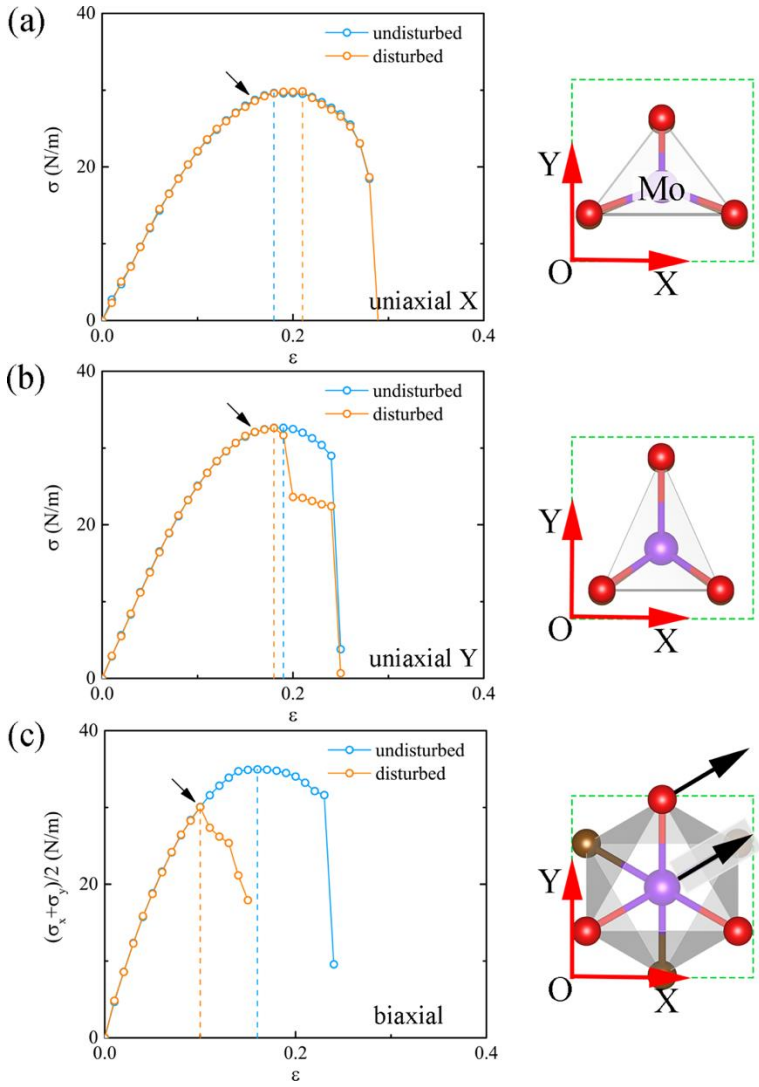

Fig. S7 The calculated stress-strain curves of Mo_2CO_2 under uniaxial tension along (a) *X* direction and (b) *Y* direction, and (c) under biaxial tension, respectively. Note that the words "undisturbed" and "disturbed" represent that the undisturbed and disturbed methods, respectively. The arrows indicate the appearance of dynamic instabilities. The right panels show the deformed polyhedral structure of Mo_2CO_2 under the corresponding strain states.

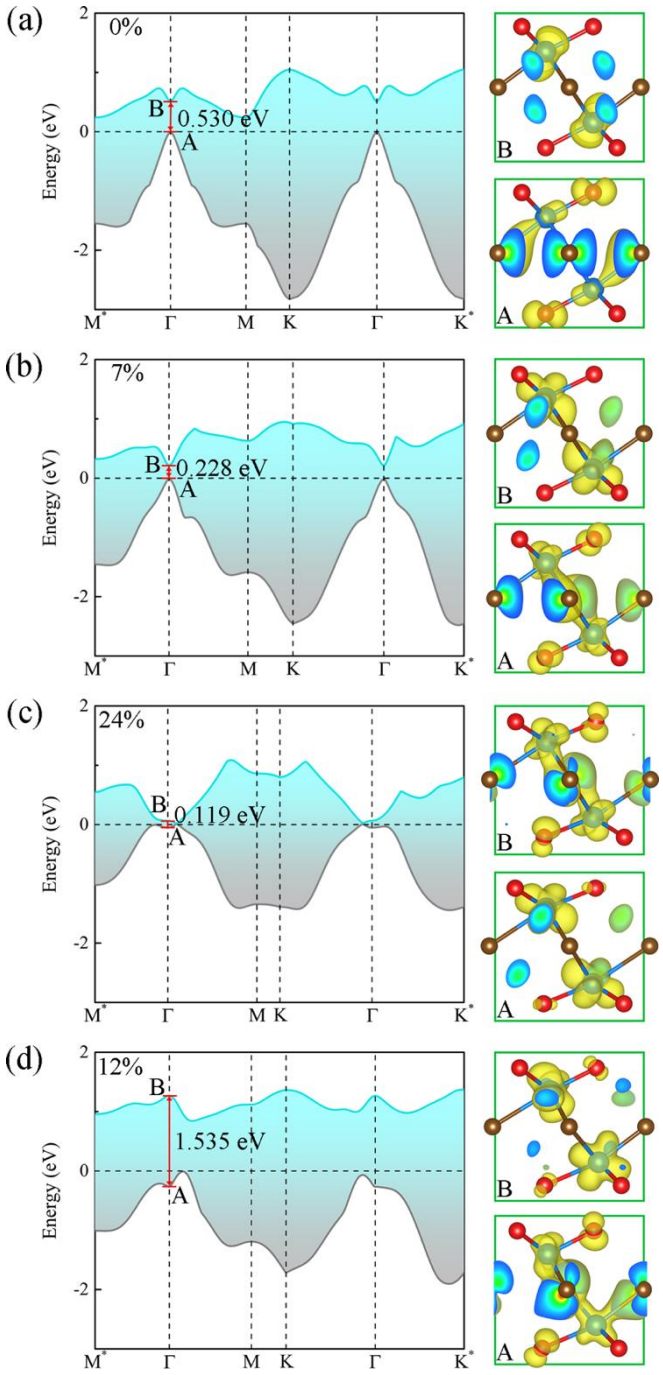

Fig. S8 The band structure of Ti_2CO_2 (a) at equilibrium ($\varepsilon = 0\%$) and at the critical strains (b) near the dynamic instability ($\varepsilon = 7\%$), (c) near the lattice instability by the undisturbed method ($\varepsilon = 24\%$), and (d) near the lattice instability by the disturbed method ($\varepsilon = 12\%$) under uniaxial tension along X direction. The Fermi level is set to zero. For clarity, only most relevant two bands near the Fermi level are drawn. The right panels show the band composed charge density (BCCD) of the two bands at Γ point projected in (110) plane. The isosurface maps of the BCCD correspond to 0.01 electrons/$Bohr^3$.

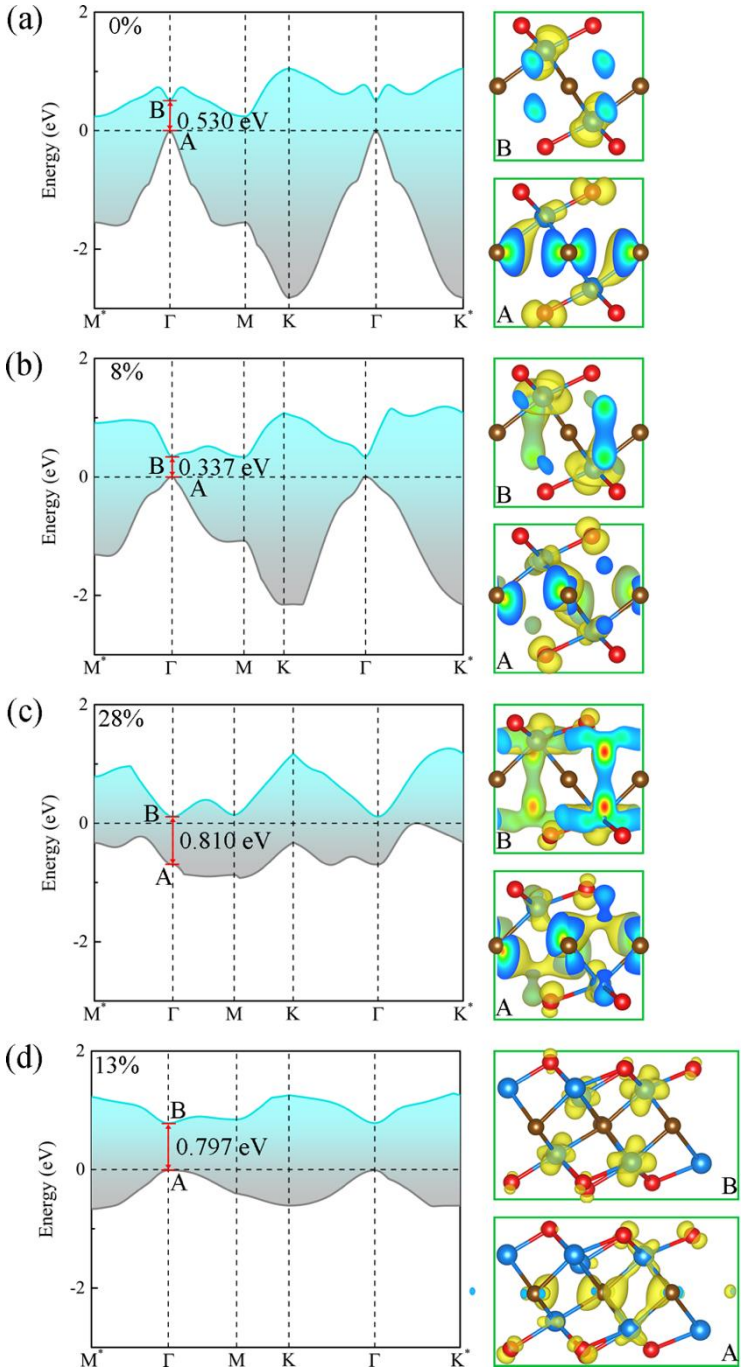

Fig. S9 The band structure of Ti_2CO_2 (a) at equilibrium ($\varepsilon = 0\%$) and at the critical strains (b) near the dynamic instability ($\varepsilon = 8\%$), (c) near the lattice instability by the undisturbed method ($\varepsilon = 28\%$), and (d) near the lattice instability by the disturbed method ($\varepsilon = 13\%$) under uniaxial tension along *Y* direction. The Fermi level is set to zero. For clarity, only most relevant two bands near the Fermi level are drawn. The right panels show the band composed charge density (BCCD) of the two bands at Γ point projected in (110) plane. The isosurface maps of the BCCD correspond to 0.01 electrons/Bohr^3.

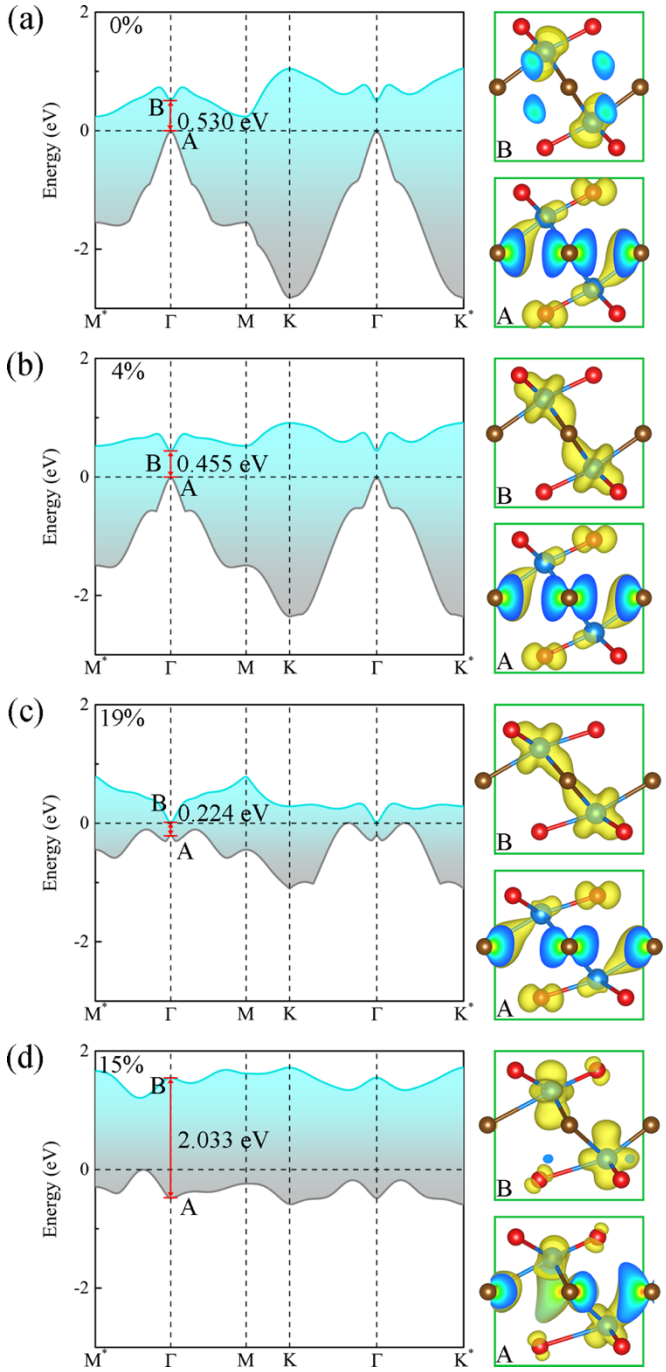

Fig. S10 The band structure of Ti_2CO_2 (a) at equilibrium ($\varepsilon = 0\%$) and at the critical strains (b) near the dynamic instability ($\varepsilon = 4\%$), (c) near the lattice instability by the undisturbed method ($\varepsilon = 19\%$), and (d) near the lattice instability by the disturbed method ($\varepsilon = 15\%$) under biaxial tension. The Fermi level is set to zero. For clarity, only most relevant two bands near the Fermi level are drawn. The right panels show the band composed charge density (BCCD) of the two bands at Γ point projected in (110) plane. The isosurface maps of the BCCD correspond to 0.01 electrons/$Bohr^3$.

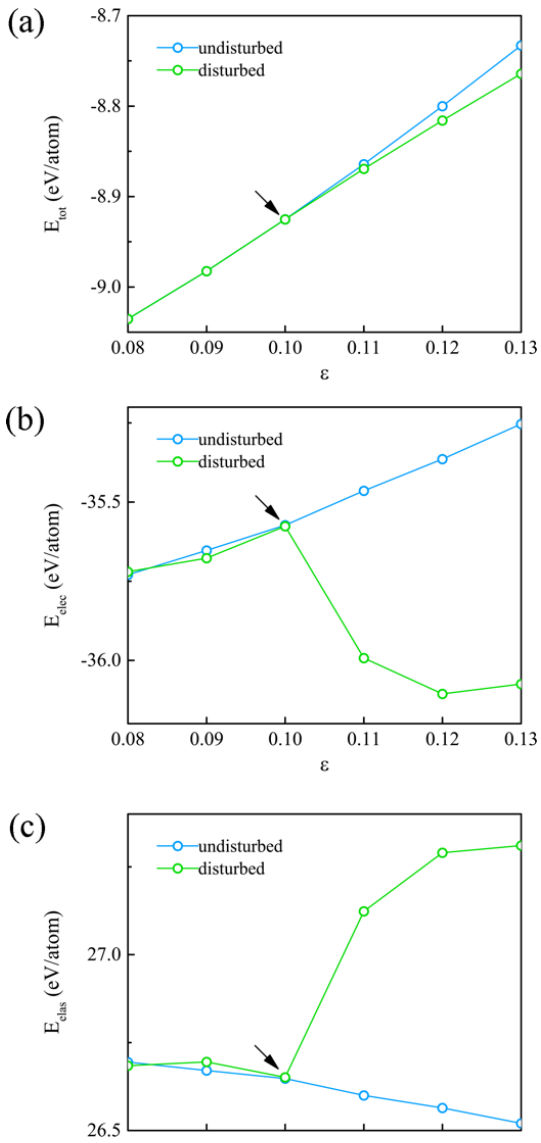

Fig. S11 (a) The total energy (E_{tot}) vs strain (ε) curves, (b) the electronic band energy (E_{elec}) vs strain (ε) curves, and (c) the elastic energy (E_{elas}) vs strain (ε) curves of metallic Mo_2CO_2 in the undisturbed mode and disturbed mode under biaxial tension. The arrows indicate the appearance of dynamic instabilities.

References

1. M. Khazaei, M. Arai, T. Sasaki, C. Y. Chung, N. S. Venkataramanan, M. Estili, Y. Sakka and Y. Kawazoe, *Adv. Funct. Mater.*, 2013, **23**, 2185-2192.
2. Y. Xie and P. R. C. Kent, *Phys. Rev. B*, 2013, **87**, 235441.
3. X. Zhang, X. Zhao, D. Wu, Y. Jing and Z. Zhou, *Nanoscale*, 2015, **7**, 16020-16025.
4. X.-H. Zha, K. Luo, Q. Li, Q. Huang, J. He, X. Wen and S. Du, *EPL (Europhysics Letters)*, 2015, **111**, 26007.
5. M. Khazaei, M. Arai, T. Sasaki, M. Estili and Y. Sakka, *Phys. Chem. Chem. Phys.*, 2014, **16**, 7841-7849.
6. J.-J. Zhang and S. Dong, *J. Chem. Phys.*, 2017, **146**, 034705.
7. H. Weng, A. Ranjbar, Y. Liang, Z. Song, M. Khazaei, S. Yunoki, M. Arai, Y. Kawazoe, Z. Fang and X. Dai, *Phys. Rev. B*, 2015, **92**, 075436.
8. F. Liu, P. Ming and J. Li, *Phys. Rev. B*, 2007, **76**, 064120.
9. C. Si, W. Duan, Z. Liu and F. Liu, *Phys. Rev. Lett.*, 2012, **109**, 226802.